

Prediction of Novel TRPV1 Antagonist: A Combination of 3D-QSAR, Molecular Docking, MD Simulations and ADMET Prediction

A. Toughzaoui^{a,*}, Ou. Chedadi^a, A. El Aissouq^{b,*}, Y. El Ouardi^c, M. Bouachrine^d and A. Ouammou^a

^aLIMOME Laboratory. Faculty of Sciences Dhar El Mahraz. Sidi Mohamed Ben Abdellah University. Fez. Morocco

^bLaboratory of Processes. Materials and Environment (LPME). Faculty of Science and Technology. Sidi Mohamed Ben Abdellah University. Fez. Morocco

^cLaboratory of Separation Technology. Lappeenranta University of Technology. Lappeenranta. Finland

^dMCNS Laboratory. Faculty of Sciences. Moulay Ismail University. Meknes. Morocco

(Received 20 March 2022, Accepted 29 June 2022)

TRPV1 are ion channels capable of sensing different stimuli, integrating and translating them into signal language. TRPV1 antagonists have attracted much attention for the treatment of various diseases, due to their properties for the management of pain physiology and neurogenic inflammation such as anti-inflammatory, antineoplastic, and anti-nociceptive. Here, we performed a three-dimensional quantitative structure-activity relationship (3D-QSAR), molecular docking, and molecular dynamics (MD) simulation on a novel series of indole triazole derivatives as antagonists of TRPV1. The aim was to design novel potent TRPV1 antagonists with strong inhibitory activity. The significant 3D-QSAR models showed a good correlation between experimental and predicted activity. Comparative molecular similarity index analysis (CoMSIA) was used to construct the best 3D-QSAR model using the PLS method with correlative and predictive ability ($R^2 = 0.985$. $Q^2 = 0.788$. $SEE = 0.105$). Electrostatic, steric, and hydrophobic fields played an important role in the variation of biological activity of the three main components. Molecular Docking analysis was used to validate the 3D-QSAR methods and explain the binding site and interactions between the most active ligands and the receptor. Based on these results, a novel series of compounds were predicted. The pharmacokinetic properties of predicted compounds were analysed by drug-likeness and ADMET prediction. The best-docked compounds were studied by MD simulation to affirm the final candidate molecules' conformational feature to confirm their dynamic behavior and stability.

Keywords: 3D-QSAR, Molecular docking, Molecular dynamic simulation, TRPV1 antagonist, Indole triazole

INTRODUCTION

The TRPV1 ion channel is a non-selective polymodal cellular receptor that allows Ca^{2+} ions to enter and receive exogenous stimuli such as capsaicin [1], resiniferatoxin, heat [2], acid [3], and mechanical stress [4], or endogenous stimuli such as the pro-inflammatory cytokine, anandamide, oxidative metabolites, and linoleic acid [5]. TRPV1 is an important link between the extracellular environment and the

cellular response by integrating and translating these stimuli into the language of calcium-based signals [4].

Recent studies have focused on TRPV1 expressed on cells of the immune system and in several types of cancer, making it a potential target for treating different disorders such as inflammation, autoimmune diseases, and cancer [5]. Its activation [6] has been implicated in neural pathophysiology (chronic inflammatory pain, peripheral neuropathology) and non-neural diseases (cystitis and asthma) [7,8,5].

TRPV1 antagonists have attracted a great deal of attention for the treatment of various diseases, specifically

*Corresponding author. E-mails: abdellah.elaissouq@usmba.ac.ma; abdelilah.toughzaoui@usmba.ac.ma

those that are related to the management of pain physiology and neurogenic inflammation [9]. Various structural classes of TRPV antagonists have been discovered; some of which have reached clinical trials. However, due to undesirable side effects such as hyper-thermic and analgesic effect, there are challenges in drug development programs [10]. This was the basis of several recent studies showing that the complete blockade of all modes of TRPV1 activation can cause hyper-thermia [11]. Indeed, many different molecular structures of antagonists selectively inhibit the capsaicin-induced TRPV1 and partially block the TRPV1 activation [12,13]. Most studies of TRPV1 antagonists are searching for a different class of antagonists that can function in a particular mode of action by selective blocking of the capsaicin-induced response to alleviate the hyper-thermic effect [11,9].

One of the strategies widely used in the medicinal chemistry programme is the chemical modification of natural compounds [14] to serve as ligands that can interact with a given receptor. Natural compounds such as rutaecarpine [15] and evodiamine [15] have shown several anti-inflammatory, antineoplastic, anti-diabetic and thermoregulatory biological effects, some of which are related to TRPV1 [15]. Moreover, voacangin, a natural product derived from tryptamine [2], is a selective stimulus antagonist that competitively inhibits the TRPV1 activated by capsaicin and heat [16]. These potent antagonists share the structural feature of 2.3.4 indole, which is the basic pharmacophore for TRPV1 inhibitory activity [17] [14]; it serves as ligands that can interact with a given receptor.

3D-QSAR is one of the computational approaches used in computer-aided drug design that aim to minimize the time and financial burden associated with the drug discovery process [18]. The research in the field of pharmaceutical industry has been developed considerably with modern pharmaceutical chemistry. 3D QSAR, molecular docking, and dynamic molecular simulation contribute efficiently and selectively in drug discovery. Molecular docking is designed to find the correct conformation of a ligand and its receptor [19,20,21]. The objective of this technique is to generate a complete set of conformations of the receptor complex and then to rank them according to their stability. The pharmacokinetic properties of the predicted compounds were analyzed by drug-likeness and ADMET prediction [22]. Molecular dynamics simulations [21] are one of the most versatile and applied computational techniques for studying

biological macromolecules, and are very useful for understanding the dynamic behaviour of proteins on different time scales [23].

In this paper, the 3D QSAR as well as molecular docking MD simulation, absorption, distribution, metabolism, excretion, and toxicity (ADMET) prediction approaches [24,25] were applied on a novel series of 2.3.4.9-tetrahydro-1H-pyrido [3.4-b] indole triazole derivatives as antagonists of TRPV1. The objective is to predict new TRPV1 antagonist inhibitors with high potency activity.

MATERIALS AND METHODS

Biological Data Set

The database used in this study is composed of 30 derivatives of 2.3.4.9-tetrahydro-1H-pyrido [3.4-b] indole triazole, which extracted from the literature with their biological activity (IC_{50}) [26]. The IC_{50} values (concentration needed to inhibit 50% of TRPV1 antagonist activity) were converted into pIC_{50} according to the formula:

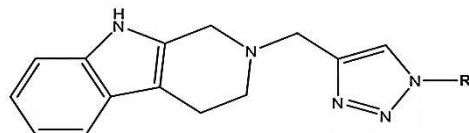
$$pIC_{50} = -\log(IC_{50} \times 10^{-6})$$

The dataset of compounds was devised in two groups: a training set of 24 molecules and a test set of 6 molecules. All compounds were visualized and optimized using ChemOffice and SYBYL-X 2.0 program package. The chemical structures and their corresponding biological data are presented in Table 1.

3D-QSAR

Molecular alignment. The optimized structures and molecular calculations were performed using sybyl software [27]. The geometries of all compounds were optimized using a conjugate gradient procedure based on the Tripos force field [28] with a convergence criterion of $0.001 \text{ kcal mol}^{-1} \text{ \AA}^{-1}$ and a maximum number of 5000 iterations. Partial atomic charges were added using Gasteiger-Hückel charges subsequently [29,30]. The compound M10 was used as a template to align the training set using the database alignment option in SYBYL-X 2.0. Each analogue was aligned on the template by rotation and translation, in order to minimize the RMSD between the atoms in the template. The alignment is shown in Fig. 1.

Table 1. Dataset of 2.3.4.9-Tetrahydro-1H-pyrido [3.4-b] Indole Triazole Derivatives with their Corresponding Experimental Activity



Compounds	R	IC ₅₀ (μ M)	pIC ₅₀	Compounds	R	IC ₅₀ (μ M)	pIC ₅₀
M1 ^T		0.314	6.503	M16 ^T		1.217	5.914
M2		2.156	5.666	M17		1.195	5.922
M3		3.489	5.457	M18		0.121	6.917
M4		0.243	6.614	M19		0.788	6.103
M5		0.416	6.380	M20		1.674	5.776
M6		0.495	6.305	M21		0.394	6.404
M7		0.232	6.634	M22		0.341	6.467
M8 ^T		0.385	6.414	M23		1.543	5.811
M9		0.494	6.306	M24		1.122	5.950
M10		0.075	7.125	M25		0.112	6.950
M11 ^T		0.089	7.050	M26		22.573	4.646
M12		0.204	6.690	M27		19.416	4.711
M13		0.108	6.966	M28		4.945	5.305
M14		2.531	5.596	M29 ^T		12.572	4.900
M15		1.878	5.726	M30		27.071	4.567

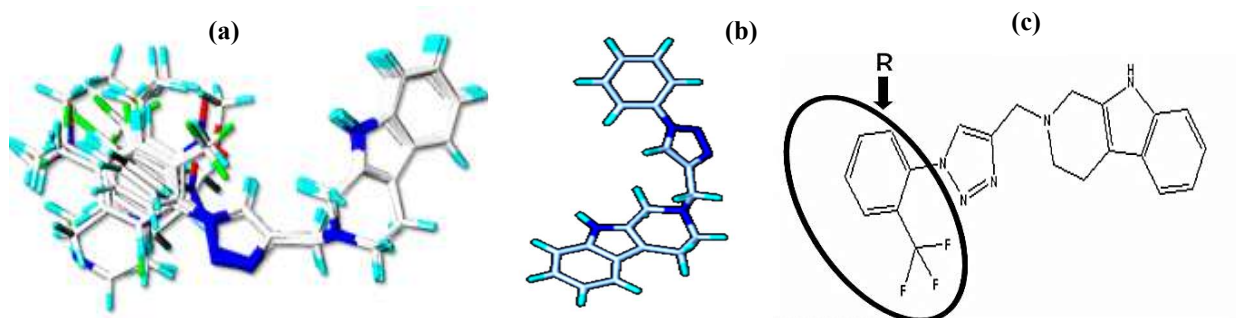


Fig. 1. Molecular alignment of data set compounds: (a) Alignment of training set compounds on the template (M10), (b) Molecular common core, and (c) Template.

CoMFA and CoMSIA analysis. Comparative Molecular Field Analysis (CoMFA) is an alignment-dependent, ligand-based molecular field method [29] that helps to establish the quantitative relationship between molecular structures and their response properties [31]. The method focuses mainly on ligand properties, such as steric and electrostatic properties and the resulting favourable and unfavourable receptor-ligand interactions. As CoMFA is an alignment-dependent descriptor-based method, all aligned ligands are inserted into an energy grid and the energy is calculated by placing an appropriate probe at each point of the grid. The resulting energy calculated at each unit fraction corresponds to the electrostatic (Columbic) and steric (van der Waals) properties. These calculated values are used as descriptors for model development. The values of these descriptors are then correlated with the biological responses using a robust linear regression method such as partial least squares (PLS) [32]. The results of the PLS method are an important signal for identifying the favourable and unfavourable electrostatic and steric potential, and for its correlation with the biological responses.

Comparative Molecular Similarity Index Analysis (CoMSIA) is a ligand-based method. Alignment-dependent linear 3D-QSAR method is an improved version of CoMFA [33]. The two mentioned approaches are almost similar except for the molecular similarity, which is also calculated in the case of CoMSIA. To compensate this, Gaussian potentials are exploited in CoMSIA fields [33], which are much smoother than the CoMFA functions. The usual energy grid box is created and similar probes are positioned throughout the grid network. In addition, the solvent-dependent molecular entropy (hydrophobicity) term is also included in CoMSIA. To analyse the property of a molecule in a data set, a common probe is placed and the similarity at

each grid point is calculated. The calculation is mainly performed on steric, electrostatic, hydrophobic, hydrogen bond acceptors and hydrogen bond donors. The mentioned properties are calculated at regularly spaced grid points corresponding to a particular descriptor that are significantly correlated with the biological response.

PLS analysis. Partial Least Squares (PLS) [29] is an extension of multiple regression analysis, was used to correlate the CoMFA and CoMSIA fields with pIC_{50} values. The CoMFA and CoMSIA descriptors were used as independent variables. While pIC_{50} values were selected as dependant variable. The Column filtering was made at the default value of 2.0 kcal mol⁻¹ in the cross-validation part and at the energy cut-off 30 kcal mol⁻¹.

The cross-validation analysis was performed using the LOO (leave-one-out) method in which one molecule was excluded from the data set. The activity of the excluded molecule was then predicted using the model derived from the rest of the data set. The leave one out cross validation method is applied to determine the correlation coefficient Q^2 and the optimal number of components (ONC).

$$Q^2 = 1 - \frac{\sum_{i=1}^{training} (Y_{iobs} - Y_{ipred})^2}{\sum_{i=1}^{training} (Y_{iobs} - \bar{Y})^2}$$

Where Y_{iobs} and Y_{ipred} are the observed and predicted values of activity, respectively. \bar{Y} is the averaged value of the activity of the training set.

The best 3D QSAR model is determined based on the values of Q^2 and R^2 , considering ($Q^2 > 0.5$) and ($R^2 > 0.6$) with low values of the standard error of estimation. The external validation was done using six molecules as a test set to estimate the predictive ability of the 3D-QSAR model

based on the value of R^2_{test} when ($R^2_{\text{test}} > 0.6$).

$$R^2_{\text{Test}} = 1 - \frac{\sum_{i=1}^{\text{test}} (Y_{i\text{obs}(\text{test})} - Y_{i\text{pred}(\text{test})})^2}{\sum_{i=1}^{\text{training}} (Y_{i\text{obs}(\text{test})} - \bar{Y}_{i\text{training}})^2}$$

Here, $Y_{i\text{obs}(\text{test})}$ and $Y_{i\text{pred}(\text{test})}$ indicate observed and predicted values of the test set compounds, respectively. $\bar{Y}_{i\text{training}}$ indicates the mean activity value of the training set.

Molecular Docking

Molecular docking [34] was applied to evaluate and study the interaction modes of a ligand derived from 2.3.4.9-tetrahydro-1H-pyrido[3.4-b]indole triazole and a receptor protein. Practically, the crystal structure of the TRPV1 protein in complex with capsaicin was obtained from the protein data bank (PDB code: 5IS0). Autodock software tools was used to determine the docking area by selecting a rectangular parallelepiped grid box of coordinates ($x = 40$, $y = 74$, $z = 44$ at 0.375) centred on the active site of protein. The visualisation of results was done using Discovery Studio 2017 R2 software. The superposition between reference and redocked ligand is shown in Fig. 2.

Molecular Dynamics (MD) Simulations

After performing the molecular docking study, the best-scored complexes were then studied by MD simulations. All the calculations were performed using the GROMACS version (2020.1-1) [35]. The topology file of each compound was created by the CHARMM General Force Field (CGenFF) server [36], while the protein topology was created by 'pdb2gmx' script. The simulations were run using the CHARMM36 all-atom (March 2019) force field [37] in a triclinic box with a distance of 1.0 nm and a TIP3P water model solvated system [38]. The neutralization of the system was performed by adding sodium or chloride (Na^+/Cl^-) ions. The energy minimization of each system was set to 50,000 steps using the steepest descent algorithm. Then, the production of MD simulation was run for 5 ns for each simulation at a temperature of 300 k, a pressure of 1 bar, and a time step of 2 fs.

RESULT AND DISCUSSION

3D-QSAR Model Analysis

The statistical results of CoMFA and CoMSIA models are presented in Table 2.

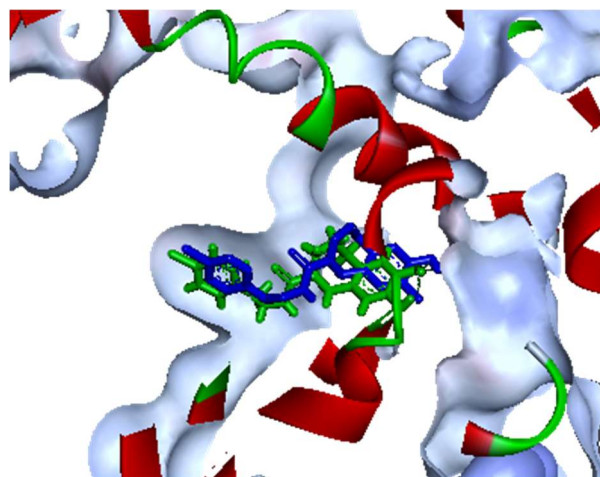


Fig. 2. Superposition of the reference ligand on the TRPV1 pocket. The blue stick represents the redocked ligand and the green stick represents the reference ligand.

Table 2. Statistical Analysis of CoMFA and CoMSIA Models using PLS Method

Parameters	ComFA	ComSIA
Q ²	0.695	0.788
R ²	0.971	0.985
ONC	5	4
SEE	0.117	0.105
R ² test	0.829	0.878
F value	149.6	187.52
Steric	0.473	0.105
Electrostatic	0.527	0.408
Hydrophobic	*	0.487
H-B Donor	*	*
H-B Acceptor	*	*

R²: Non-cross-validated correlation coefficient; Q²: Cross-validated correlation coefficient; SEE: Standard error of the estimate; N: Optimum number of components; R²_{test}: External validation correlation coefficient; F: F-test value.

Considering the CoMFA model, the partial least square (PLS) regression gave a cross-validated correlation coefficient $Q^2 = 0.695 > 0.5$ with an optimal number of components equal to 6, which shows that the model is reliable for the prediction of the pIC₅₀ values. The non-validated PLS analysis gave a high correlation coefficient (R^2) value of 0.971, a low standard error estimate (SEE) of 0.117, and an

F-value of 149.6. The contribution of steric field was 0.473 while that of electrostatic field was 0.527. The test set correlation coefficient had the value of $R^2_{\text{test}} = 0.829$. The experimental and predicted pIC_{50} values of the training set compounds and the test set compounds and the residual values are shown in Table 3.

The graph showing the actual values of pIC_{50} as a function of the predicted values of the CoMFA model is shown in Fig. 3 in which almost all the points are located on the diagonal line.

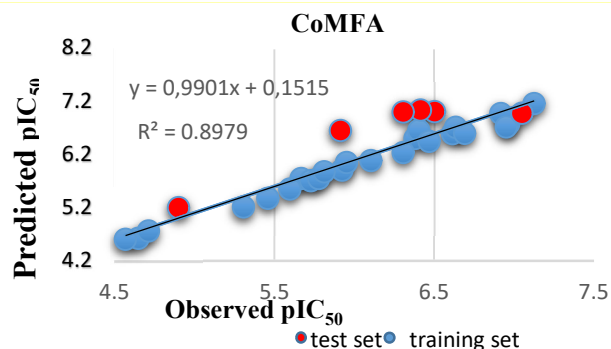


Fig. 3. Correlation plot of CoMFA between the experimental and predicted activities.

Table 3. Observed, Predicted Activity, and Residual Values Obtained by CoMFA and CoMSIA Models

Compounds	pIC_{50}	CoMFA	Residual	CoMSIA	Residual
M1 ^t	6.503	7.003	-0.5	6.154	0.349
M2	5.666	5.751	-0.085	5.673	-0.007
M3	5.457	5.377	0.08	5.505	-0.048
M4	6.614	6.597	0.017	6.633	-0.019
M5	6.38	6.504	-0.124	6.46	-0.08
M6	6.305	6.238	0.067	6.146	0.159
M7	6.634	6.714	-0.08	6.657	-0.023
M8 ^t	6.414	7.028	-0.614	6.463	-0.049
M9 ^t	6.306	6.996	-0.69	6.433	-0.127
M10	7.125	7.158	-0.033	7.097	0.028
M11 ^t	7.05	6.97	0.08	6.618	0.432
M12	6.69	6.602	0.088	6.664	0.026
M13	6.966	6.779	0.187	6.723	0.243
M14	5.596	5.556	0.04	5.616	-0.02
M15	5.726	5.71	0.016	5.745	-0.019
M16 ^t	5.914	6.644	-0.73	6.087	-0.173
M17	5.922	5.907	0.015	5.95	-0.028
M18	6.917	6.975	-0.058	6.939	-0.022
M19	6.103	6.09	0.013	6.009	0.094
M20	5.776	5.751	0.025	5.781	-0.005
M21	6.404	6.656	-0.252	6.661	-0.257
M22	6.467	6.45	0.017	6.455	0.012
M23	5.811	5.876	-0.065	5.82	-0.009
M24	5.95	6.051	-0.101	5.937	0.013
M25	6.95	6.722	0.228	6.975	-0.025
M26	4.646	4.625	0.021	4.575	0.071
M27	4.711	4.768	-0.057	4.796	-0.085
M28	5.305	5.219	0.086	5.331	-0.026
M29 ^t	4.9	5.197	-0.297	4.762	0.138
M30	4.567	4.612	-0.045	4.543	0.024

^tRepresents the test set compounds.

In the CoMSIA model, the statistical parameters were improved and it was obtained that the steric, electrostatic and hydrophobic fields influenced the antagonistic activity of TRPV1 in a significant way. It gave a cross-validated correlation coefficient of $Q^2 = 0.788$ with an optimal component number of 4, a correlation coefficient $R^2 = 0.985$, a low standard error estimate of 0.105, and an F-value of 187.52. The relative contributions were 0.105, 0.408, and 0.487 for the steric, electrostatic, and hydrophobic fields, respectively. The predictive correlation coefficient of the test set had a value of $R^2_{\text{test}} = 0.878$. The experimental and predicted pIC_{50} values for the training set and test set data are shown in Table 2. The plot of the experimental activity versus the predicted pIC_{50} activity is shown in Fig. 4 with all points located on the diagonal line.

Interpretation of CoMFA and CoMSIA Contours

The contour map visualized the results of the CoMFA and CoMSIA model and showed the regions of 3D space where molecular fields predominate, vary, and helps to identify sites where changes in molecular fields are strongly correlated with concurrent changes in biological activity.

CoMFA contour maps. The contour map of the CoMFA model molecular fields of the most active compound M10 is shown in Fig. 6. The steric field was represented by green contours, which highlighted the regions where the presence

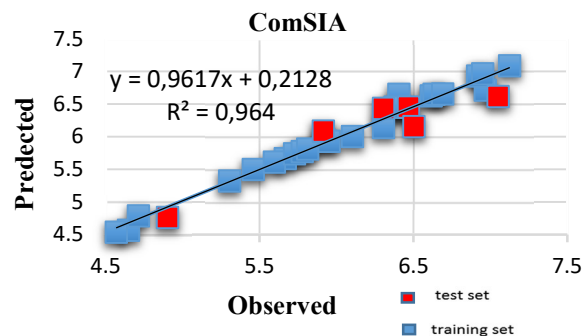


Fig. 4. Correlation plot between the experimental and predicted activities of CoMSIA model.

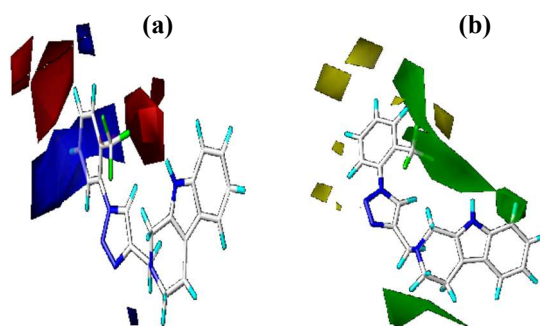


Fig. 5. Standardized coefficient Contour maps of CoMFA analysis of the TRPV1 antagonist activity (compound M10) (a) steric Contour maps; (b) electrostatic Contour maps.

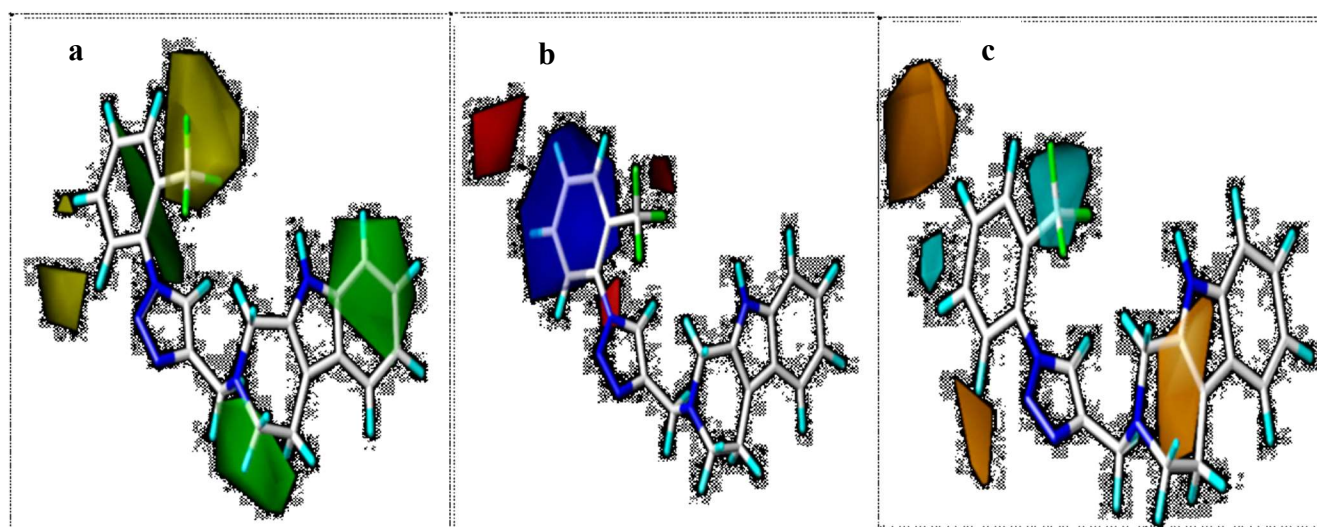


Fig. 6. Standardized coefficient Contour maps of CoMSIA analysis of TRPV antagonist activity (compound M10): (a) steric Contour maps; (b) electrostatic Contour maps; (c) Hydrophobic contour map.

of the steric bulky group is favourable for enhancing the TRPV1 antagonist activity of the compounds. As shown in Fig. 5, the most dominant green contour is in the position of the substituent R suggesting that the existence of a bulky group in this region would be favourable. This explains, for example, the activity of compounds M10 (R = phenyl-CF₃), M18 (R = phenyl-NO₂), M15 (R = phenyl-Cl) has this order: $pIC_{50} M10 = 7.125 > pIC_{50} M18 = 6.917 > pIC_{50} M5 = 6.380$. The electrostatic field was represented by blue contours; this indicates the regions where the existence of an electro-donating group in the R substituent, particularly in the 4-position of the substituted benzene, improved the activity. This further explains the increase in activity from M5, M18 to M10 while the unfavourable regions of the electrostatic field are represented by red contours.

CoMSIA contour maps. In fact, different CoMSIA models were generated using multiple combined fields. A model including the steric electrostatic and hydrophobic fields gave a higher Q² value than the CoMFA model showing that the hydrophobic field is an important factor in the antagonist activity of TRPV1. The contour map of the CoMSIA model visualised the partitioning of the steric, electrostatic and hydrophobic molecular fields on the molecular skeleton of the most active molecule (M10). The results are shown in Fig. 6. The steric field showed 10% of the global contribution of the molecular fields. The green contour shows that the presence of a bulky group at the R-substituent, specifically on the phenyl, is linked to the triazole and the indole change improving the biological activity. This explains the notable activity of the M10 compounds. M11, M2, M18, M19: $pIC_{50} M10 = 7.125$, $pIC_{50} M11 = 6.917$, $pIC_{50} M2 = 6.380$, $pIC_{50} M18 = 0.7125$, $pIC_{50} M19 = 6.917$, while the yellow contour showed the unfavourable steric field regions.

The electrostatic field represents almost 41% of the total contribution of the molecular fields. The blue contour shows the regions where the presence of an electron donor or electron acceptor group influences the biological activity. The blue contour shows the favourable areas of the electrostatic field that is located specifically in the R-substituent explaining the high activity of the compounds M10, M11, M2, M12 and M19. The red contour shows the unfavourable regions of the electrostatic field. The hydrophobic field represents almost half of the total

contribution of the molecular fields included in the model (49%), showing the crucial role of the hydrophobic fields in the antagonistic activity of TRPV1. The contour map of the most active molecule (M10) shows a cyan contour, indicating the regions that favour the presence of a hydrophobic group located in the R substituent, particular in position 2 and 5 of the substituted benzene ring linked to the triazole. This explains the high activity of M10, M2, M12 and M19. In addition, there was an orange unfavourable contour related to the hydrophobic group in position 6 of the substituted benzene ring. The latter contour is linked to the triazole indicating the improved activity when a hydrophobic group is placed in position 2 compared to positions 3 and 4; $pIC_{50} M10$ (R = phenyl-CF₃ in position 2) = 7.7125, $pIC_{50} M11$ (R = phenyl-CF₃ in position 3) = 7.05, $pIC_{50} M1$ (R = phenyl-CF₃ in position 4) = 6.906.

Design of New TRPV1 Antagonist

The design of new TRPV1 antagonists is based on the interactions generated by the 3D QSAR model and molecular docking to give a more potent and improved activity. Based on 3D-QSAR, we found that steric, electrostatic, and hydrophobic fields play important roles in the activities of the studied compounds. Indeed, we propose three new TRPV1 antagonists based on SAR information from the 3D QSAR study that are shown in Fig. 7. The chemical structure and

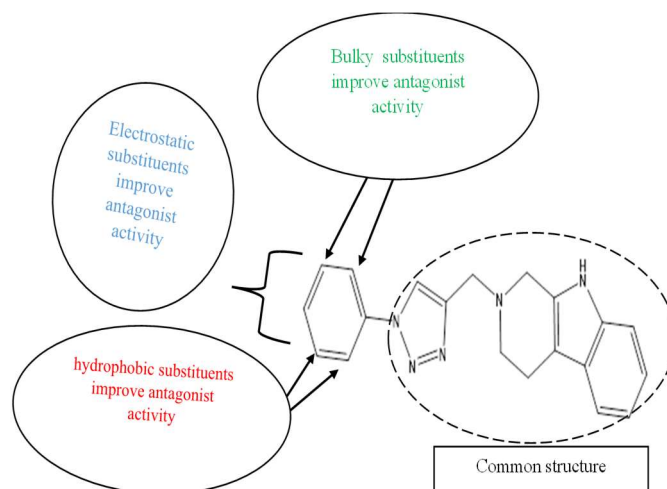


Fig. 7. Structure-activity relationship (SAR) information obtained from the 3D-QSAR study.

predicted activity values of the new compounds are presented in Table 4.

The three proposed compounds showed good predicted activities compared to the most potent antagonist. To ensure the designed compounds are good antagonists, we performed molecular docking studies on the proposed compounds, which are shown in Table 4.

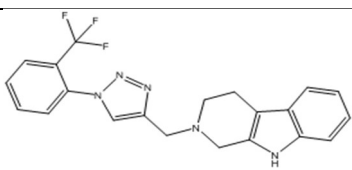
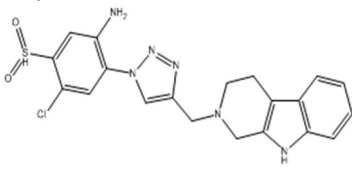
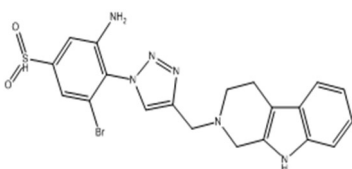
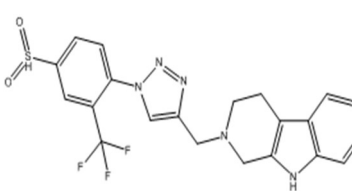
Molecular Docking Results

The docking study was performed between the (PDB ID: 5IS0) receptor and the ligands P1, P2 and P3. All compounds were docked by occupying the active site of the target protein. The binding affinity values of the most active

compound and the proposed compounds are shown in Table 4. According to our results, the three ligands had a higher binding energy than the most potent TRPV1 antagonist did. These complexes were visualised and analysed by the Discovery Studio 2017 R2 software that are shown in Figs. 8, 9, 10 and 11.

The difference between the binding affinity values of the complexes is proportional to the stability of the protein-ligand interaction; all tested ligands have the potential to establish strong and stable complexes with the target protein [21]. The results of the binding site interactions of compound M10 and TRPV1 antagonist receptor (PDB ID: 5IS0) is presented in Fig. 8. As shown, compound M10 formed

Table 4. The Binding Energy Values of the most Active Compound and the Proposed Compounds

Compounds	Binding (kcal mol ⁻¹)	pIC ₅₀
	-8.95	7.125
M10		
	-9.02	7.126
P1		
	-9.32	7.370
P2		
	-9.27	7.364
P3		

four hydrogen bonds with GLU C: 513, TYR C: 495, TYR C: 554, and SER C: 510. It also had three hydrophobic interactions with ARG C: 491, ILE C: 703, SER: 501, and three electrostatic interactions with ARG C: 557, ARG C: 491, GLU C 513. The most active predicted molecule P2 formed more hydrogen bonds than the M10, P1 and P3

compounds. P2 formed seven hydrogen bonds with TYR C: 511, ALA C: 566, LEU C: 553, THR C: 556 ARG C: 557, THR C: 550, and TYR C: 554. It also had three hydrophobic interactions with ILE C: 573, ALA C: 566, and LEU C: 553, and an electrostatic interaction with GLU C: 570. This type of interaction are signs of ligand docking in favourable

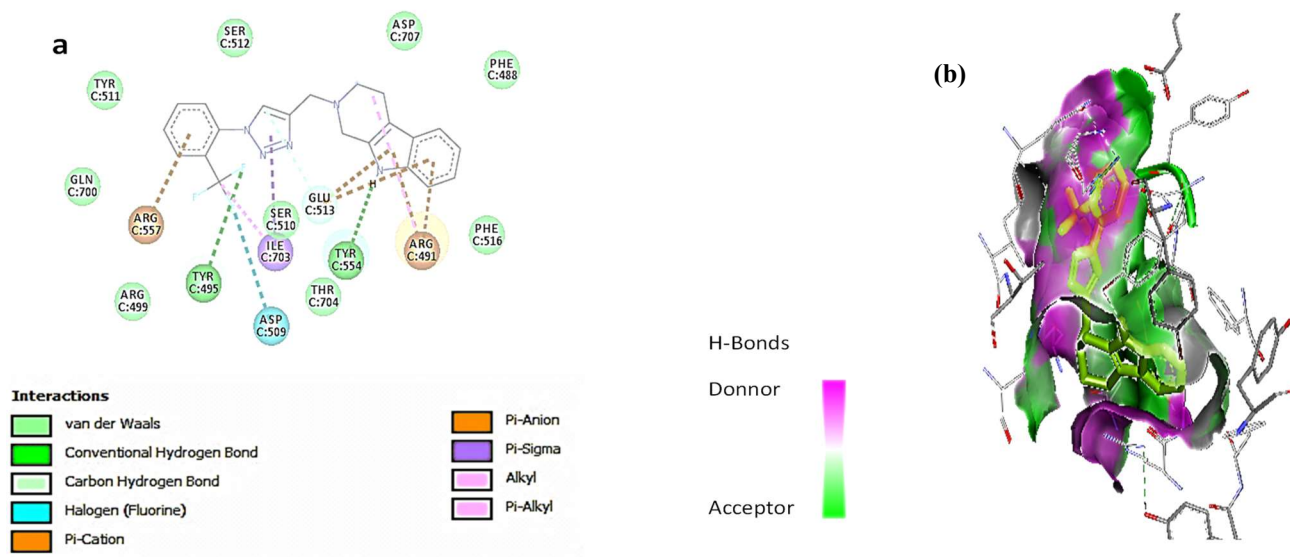


Fig. 8. Molecular docking of antagonist M10 with (PDB ID: 5IS0) protein. (a) Binding site interactions of 2D view. (b) Hydrogen binding conformation of 3D view.

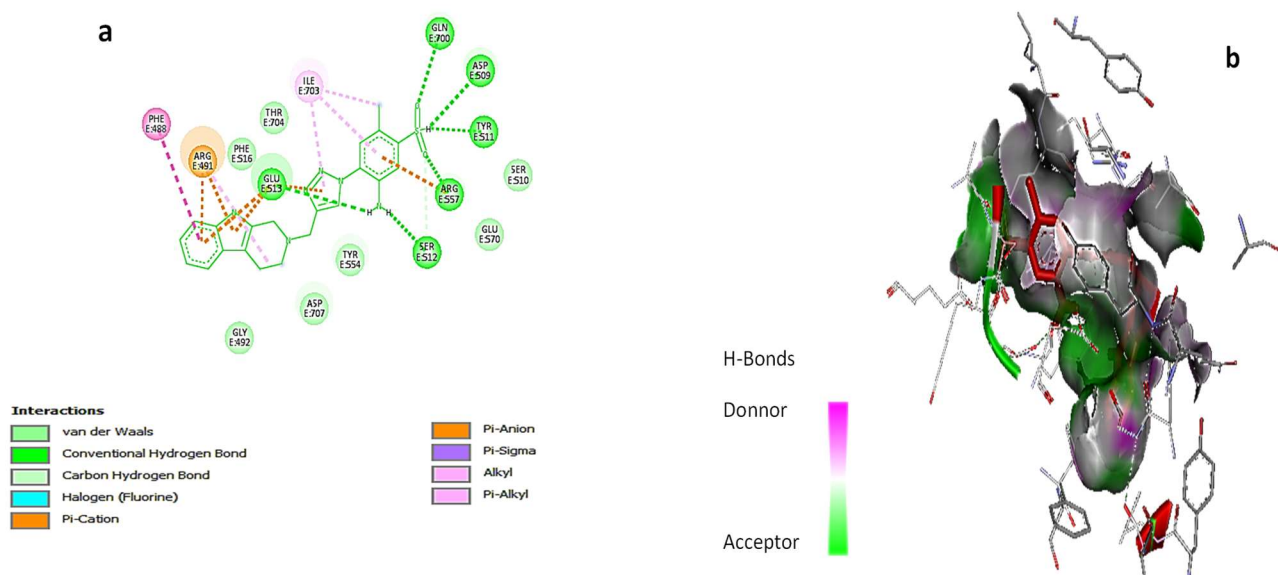


Fig. 9. Molecular docking of antagonist P1 with (PDB ID: 5IS0) protein. (a) Binding site interactions of 2D view. (b) Hydrogen binding conformation of 3D view.

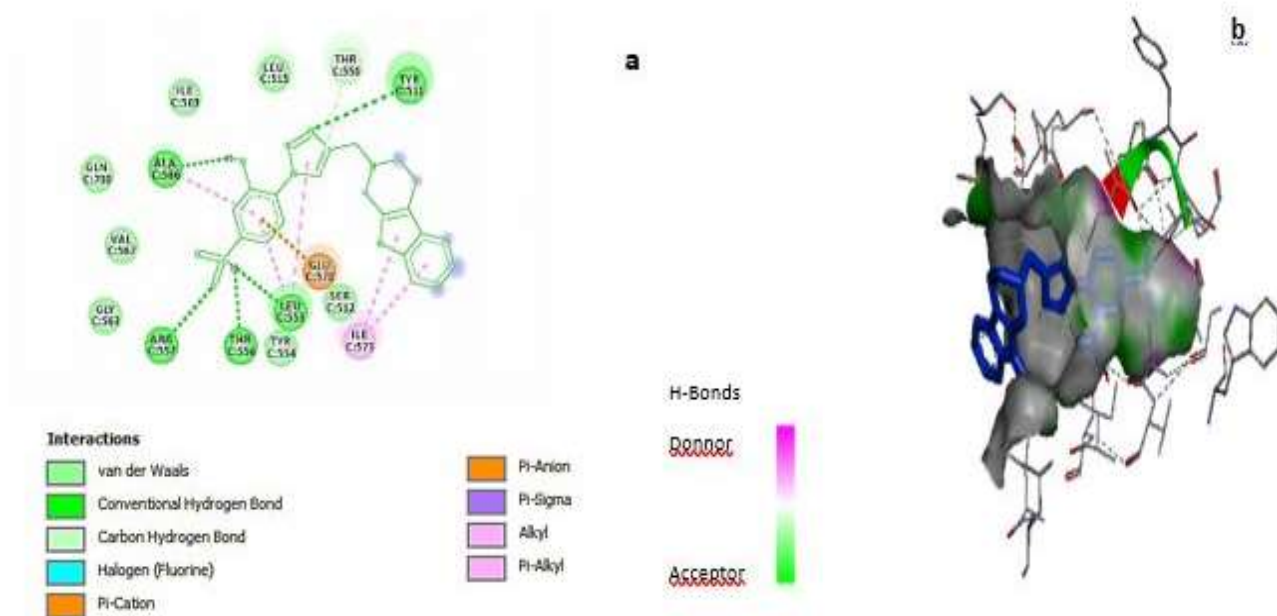


Fig. 10. Molecular docking of antagonist P2 with (PDB ID: 5IS0) protein. (a) Binding site interactions of 2D view. (b) Hydrogen binding conformation of 3D view.

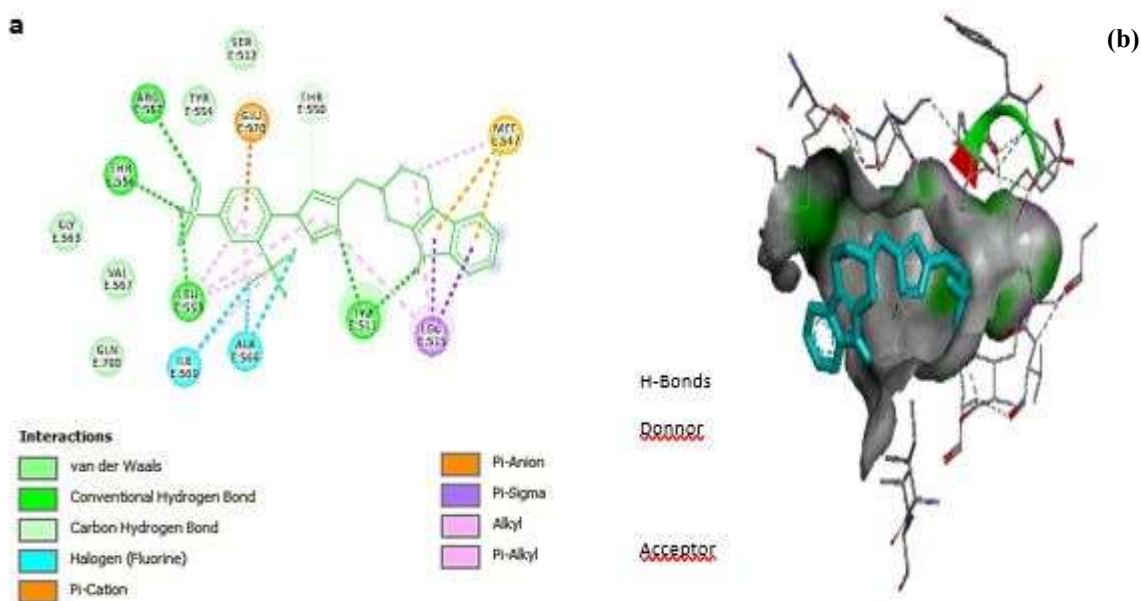


Fig. 11. Molecular docking of antagonist P3 with (PDB ID: 5IS0) protein. (a) Binding site interactions of 2D view. (b) Hydrogen binding conformation of 3D view.

contributors to stability. Electrostatic interactions are generally associated with binding affinity to the structure as well as biological reactivity of the proteins and nucleic acids [40], showing that P2 could have these different interactions.

Predicted compounds P1 and P3 also formed hydrogen bonds, hydrophobic interactions, and electrostatic interactions with the receptor. The results are shown in Table 5.

Table 5. Interactions of Amino acid Residues with Ligands at Receptor Sites

Ligands	Hydrogen-binding interaction	Hydrophobic interaction	Electrostatic interaction	Ligands	Hydrogen-binding interaction	Hydrophobic interaction	Electrostatic interaction
P10	GLU C: 513		ARG C: 557	P2	TYR C: 511		
	TYR C: 495	ARG C: 491	ARG C: 491		ALA C: 566		
P1	TYR C: 554	ILE C: 703	GLU C: 513	LEU C: 553	ILE C: 573		GLU C: 570
	SER C: 510	SER C: 501		THR C: 556	ALA C: 566		
P1				ARG C: 557	LEU C: 553		
	GLU E: 700			THR C: 550	TYR C: 554		
P1	ASP E: 509		ARG E: 491	ARG E: 557			
	TYR E: 511	ILE E: 703	ARG E: 557	THR E: 556	LEU E: 515		GLU E: 570
P1	ARG E: 557	PHE E: 488	GLU E: 513	LEU E: 553	ALA E: 566		MET E: 547
	SER E: 512			TYR E: 511	ILE E: 589		
	GLU E: 513			THR E: 550			

Molecular Dynamics Simulation

In order to validate the molecular docking results affirm the stability of the docked compounds in the (PDB ID: 5IS0)binding pocket, compounds M10 and P1 were studied by MD simulation. All systems were assigned to a 5 ns timescale simulation. The root mean square deviation (RMSD) of the 5IS0_M10 and 5IS0_P2 complexes is given in Fig. 12 and 13. It was obtained that the mean value of the RMSD of the 5IS0_M10 and 5IS0_P2 systems were 0.19 nm and 0.11 nm, respectively. These results indicated that the 5IS0_P2 complex was more stable than the 5IS0_M10 complex during the MD simulation. These results are in agreement with those obtained by 3D-QSAR and molecular docking.

ADME/T Prediction

Before the experiment, the pharmacokinetic properties of the predicted new compounds must be tested [41]. Here, the pkCSM [42] and SwissADMET [22] web servers were used to perform ADMET (absorption, distribution, metabolism, excretion, and toxicity). The results are presented in Table 6.

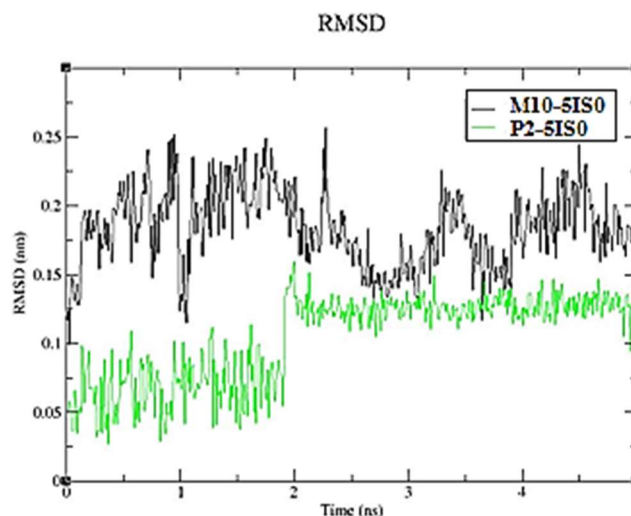


Fig. 12. Molecular dynamics simulations. RMSD of backbone over the 5 ns of MD simulation at 300 K and 1 bar.

As shown in Table 6, all predicted compounds exhibited moderate ADMET parameters. High values of human

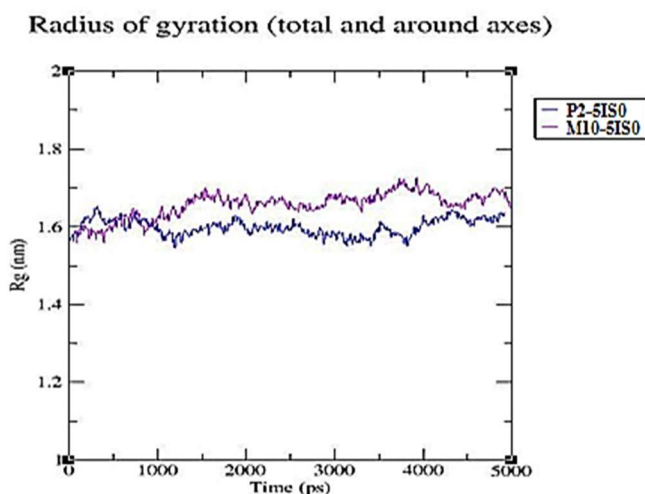


Fig. 13. RMSF of residues during MD simulation. In all figures, the blue color represents the 5IS0_M10 complex and the violet color represents the 5IS0_P2 complex.

intestinal absorption ($HIA > 30\%$) show that the predicted compounds passed through the intestinal membrane in a moderate way. High value of Caco-2 permeability ($>90\%$) of compound P1 revealed that this compound had a high Caco-2 permeability. In summary, it can be concluded that the predicted compounds are likely to be orally active. In addition, the synthetic accessibility of all predicted

compounds was close to 1, which means that these compounds are very easy to synthesize.

CONCLUSIONS

This research introduces new TRPV1 antagonist compounds from a series of compounds by application of 3D-QSAR studies, including CoMFA and CoMSIA methods. The results of the CoMFA and CoMSIA studies using PLS method showed that the resulting values of Q^2 , R^2_{test} and R^2 are very high for all models. The chemical interactions of the binding site between the ligands and the target protein were studied using molecular docking. The docking results were in agreement with the 3D-QSAR studies. Based on these studies, three new compounds (P1-3) were predicted using the CoMSIA method. The results of the docking analysis showed that, compared to the most potent antagonist in the dataset (compound M10), the predicted compounds had a high degree of stability in the protein-binding pocket. The MD simulation results also indicated that compound P2 was more stable in the receptor-binding pocket during the 5 ns simulation time.

CONFLICT OF INTEREST

All authors declare that they have no conflict of interest in this work.

Table 6. ADME/T Analysis and Synthetic Accessibility of Predicted Compounds

Compounds	Absorption			Distribution	Metabolism								Excretion	Toxicity		Synthetic
	Water solubility	Caco2 permeability	Intestinal absorption		Blood Brain	CYP								Total Clearance	AMES toxicity	
				2D6		3A4	1A2	2C19	2C9	2D6	3A4	Substrate	Inhibitor			
				Numeric (log M)		Numeric (logPapp in $10^{-6} \text{ cm s}^{-1}$)	Numeric (%) Absorbed	Numeric (logBB)	Categorical (Yes/No)							
P1	-3.59	-0.043	81.58	-1.51	Yes	Yes	Yes	No	No	No	Yes	0.90	YES	0.40	3.25	
P2	-3.60	-0.04	81.31	-1.53	Yes	Yes	Yes	No	No	No	Yes	0.86	YES	0.40	3.32	
P3	-3.81	0.98	91	-1.46	No	Yes	Yes	Yes	Yes	No	Yes	0.60	NO	0.09	3.25	
M10	-4.28	0.84	92	0.36	Yes	Yes	Yes	No	No	Yes	No	0.81	NO	0.04	3.15	

REFERENCES

- [1] Seebohm, G.; Schreiber, J. A., Beyond Hot and Spicy: TRPV Channels and Their Pharmacological Modulation. *Cellular Physiology and Biochemistry* **2021**, *22*, 108-130, DOI: 10.33594/000000358.
- [2] Loyd, D. R.; Chen, P. B.; Hargreaves, K. M., Anti-Hyperalgesic Effects of Anti-Serotonergic Compounds on Serotonin- and Capsaicin-Evoked Thermal Hyperalgesia in the Rat. *Neuroscience* **2012**, *203*, 207-215, DOI: 10.1016/j.neuroscience.2011.12.019.
- [3] Sawhney, J. P.; Kothiwale, V. A.; Bisne, V.; Durgaprasad, R.; Jadhav, P.; Chopda, M.; Vanajakshamma, V.; Meena, R.; Vijayaraghavan, G.; Chawla, K., *et al.* Risk Profiles and One-Year Outcomes of Patients with Newly Diagnosed Atrial Fibrillation in India: Insights from the GARFIELD-AF Registry. *Indian Heart J.* **2018**, *70*, DOI: 10.1016/j.ihj.2018.09.001.
- [4] Inoue, R.; Jian, Z.; Kawarabayashi, Y., Mechanosensitive TRP Channels in Cardiovascular Pathophysiology. *Pharmacol. Ther.* **2009**, *123*, 371-385. DOI: <https://doi.org/10.3934/biophy.2016.1.63>.
- [5] Csekő, K.; Beckers, B.; Keszthelyi, D.; Helyes, Z., Role of TRPV1 and TRPA1 Ion Channels in Inflammatory Bowel Diseases: Potential Therapeutic Targets? *Pharmaceuticals* **2019**, *12*, 48, DOI: <https://dx.doi.org/10.3390/2Fph12020048>.
- [6] Yin, Y.; Dong, Y.; Vu, S.; Yang, F.; Yarov-Yarovoy, V.; Tian, Y.; Zheng, J., Structural Mechanisms Underlying Activation of TRPV1 Channels by Pungent Compounds in Gingers. *British Journal of Pharmacology* **2019**, *176*, 3364-3377, DOI: 10.1111/bph.14766.
- [7] Reyes-García, J.; Carbajal-García, A.; Montaña, L. M., Transient Receptor Potential Cation Channel Subfamily V (TRPV) and Its Importance in Asthma. *European Journal of Pharmacology* **2022**, *915*, 174692, DOI: 10.1016/J.EJP.2021.174692.
- [8] Aghazadeh Tabrizi, M.; Baraldi, P. G.; Baraldi, S.; Gessi, S.; Merighi, S.; Borea, P. A., Medicinal Chemistry, Pharmacology, and Clinical Implications of TRPV1 Receptor Antagonists. *Med. Res. Rev.* **2017**, *37*, 936-983. DOI: <https://doi.org/10.1002/med.21427>.
- [9] Wong, G. Y.; Gavva, N. R., Therapeutic Potential of Vanilloid Receptor TRPV1 Agonists and Antagonists as Analgesics: Recent Advances and Setbacks. *Brain Research Reviews* **2009**, *60*, 267-277. DOI: <https://doi.org/10.1016/j.brainresrev.2008.12.006>.
- [10] Kort, M. E.; Kym, P. R., TRPV1 Antagonists: Clinical Setbacks and Prospects for Future Development. In *Progress in Medicinal Chemistry*; Elsevier B.V., **2012**, *51*, 57-70. DOI: <https://dx.doi.org/10.1016/j.pain.2008.01.024>.
- [11] Voight, E. A.; Gomtsyan, A. R.; Daanen, J. F.; Perner, R. J.; Schmidt, R. G.; Bayburt, E. K.; Didomenico, S.; McDonald, H. A.; Puttfarcken, P. S.; Chen, J., *et al.* Discovery of (R)-1-(7-Chloro-2,2-Bis(Fluoromethyl)Chroman-4-Yl)-3-(3-Methylisoquinolin-5-Yl)Urea (a-1165442): A Temperature-Neutral Transient Receptor Potential Vanilloid-1 (Trpv1) Antagonist with Analgesic Efficacy. *J. Med. Chem.* **2014**, *57*, 7412-7424, DOI: 10.1021/jm500916t.
- [12] Reilly, R. M.; McDonald, H. A.; Puttfarcken, P. S.; Joshi, S. K.; Lewis, L. G.; Pai, M.; Franklin, P. H.; Segreti, J. A.; Neelands, T. R.; Han, P., *et al.* Pharmacology of Modality-Specific Transient Receptor Potential Vanilloid-1 Antagonists That Do Not Alter Body Temperature. *J. Pharmacol. Exp. Ther.* **2012**, *342*, 416-428, DOI: 10.1124/jpet.111.190314.
- [13] Garami, A.; Shimansky, Y. P.; Pakai, E.; Oliveira, D. L.; Gavva, N. R.; Romanovsky, A. A., Contributions of Different Modes of TRPV1 Activation to TRPV1 Antagonist-Induced Hyperthermia. *J. Neurosci.* **2010**, *30*, 1435-1440, DOI: 10.1523/JNEUROSCI.5150-09.2010.
- [14] Szychowski, J.; Truchon, J. F.; Bennani, Y. L. Natural Products in Medicine: Transformational Outcome of Synthetic Chemistry. *J. Med. Chem.* **2014**, *57*, 9292-9308. DOI: <https://doi.org/10.1021/jm500941m>.
- [15] Wang, S.; Yamamoto, S.; Kogure, Y.; Zhang, W.; Noguchi, K.; Dai, Y., Partial Activation and Inhibition of TRPV1 Channels by Evodiamine and Rutaecarpine, Two Major Components of the Fruits of *Evodia Rutaecarpa*. *J. Nat. Prod.* **2016**, *79*, 1225-1230, DOI: 10.1021/acs.jnatprod.5b00599.

- [16] TRPV1 Receptors and Signal Transduction. In TRP Ion Channel Function in Sensory Transduction and Cellular Signaling Cascades; *CRC Press*. **2021**. pp. 69-84, DOI: <https://doi.org/10.1201/9781420005844>.
- [17] Terada, Y.; Horie, S.; Takayama, H.; Uchida, K.; Tominaga, M.; Watanabe, T. Activation and Inhibition of Thermosensitive TRP Channels by Voacangine, an Alkaloid Present in Voacanga Africana, an African Tree. *J. Nat. Prod.* **2014**, *77*, 285–297, DOI: 10.1021/np400885u.
- [18] Thirumurugan, P.; Matosiuk, D.; Jozwiak, K. Click Chemistry for Drug Development and Diverse Chemical-Biology Applications. *Chem. Rev.* **2013**, *113*, 4905-4979. DOI: <https://doi.org/10.1021/cr200409f>.
- [19] El Aissouq, A.; Chedadi, O.; Bouachrine, M.; Ouammou, A., Identification of Novel SARS-CoV-2 Inhibitors: A Structure-Based Virtual Screening Approach. *J. Chem.* **2021**, Article ID 1901484, 7 pages, DOI: 10.1155/2021/1901484.
- [20] Goudzal, A.; Aissouq, A. El; Hamdani, H. El; Ouammou, A. Materials Today: Proceedings QSAR Modeling, Molecular Docking Studies and ADMET Prediction on a Series of Phenylaminopyrimidine-(Thio) Urea Derivatives as CK2 Inhibitors. *Mater. Today Proc.* **2020**, DOI: 10.1016/j.matpr.2020.08.044.
- [21] Shamshad, H.; Saeed, M.; Ul-Haq, Z.; Halim, S. A.; Gul, S.; Mirza, A. Z., Relative Assessment of Different Statistical Instruments and Measures for the Prediction of Promising Outcomes Using Docking, Virtual Screening and ADMET Analysis against HIV-RT. *Journal of Biomolecular Structure and Dynamics* **2021**, *0*, 1-13, DOI: 10.1080/07391102.2021.1900915.
- [22] Daina, A.; Michielin, O.; Zoete, V. SwissADME: A Free Web Tool to Evaluate Pharmacokinetics, Drug-Likeness and Medicinal Chemistry Friendliness of Small Molecules. *Scientific Reports* **2017**, *7*, 1-13, DOI: 10.1038/srep42717.
- [23] Oussama, C., *In Silico* Prediction of Novel SARS-CoV 3CL pro Inhibitors: A Combination of 3D-QSAR , Molecular Docking, ADMET Prediction, and Molecular Dynamics Simulation. *Biointerface Res. Appl. Chem.* **2022**, *12*, 5100-5115. DOI: <https://doi.org/10.33263/BRIAC124.51005115>.
- [24] Shamshad, H.; Hafiz, A.; Althagafi, I.I.; Saeed, M.; Mirza, A.Z. Characterization of the Trypanosoma Brucei Pteridine Reductase Active- Site Using Computational Docking and Virtual Screening Techniques. *Current Computer-Aided Drug Design* **2019**, *16*, DOI: 10.2174/1573409915666190827163327.
- [25] Alonso, H.; Bliznyuk, A.A.; Gready, J.E. Combining Docking and Molecular Dynamic Simulations in Drug Design. *Med. Res. Rev.* **2006**, *26*, 531-568.
- [26] Li, J.; Nie, C.; Qiao, Y.; Hu, J.; Li, Q.; Wang, Q.; Pu, X.; Yan, L.; Qian, H. Design, Synthesis and Biological Evaluation of Novel 2,3,4,9-Tetrahydro-1H-Pyrido[3,4-b]Indole Triazole Derivatives as Potent TRPV1 Antagonists. *Eur. J. Med. Chem.* **2019**, *178*, 433-445, DOI: 10.1016/j.ejmech.2019.06.007.
- [27] Tong, L.; Guo, L.; Lv, X.; Li, Y., Modification of Polychlorinated Phenols and Evaluation of Their Toxicity, Biodegradation and Bioconcentration Using Three-Dimensional Quantitative Structure-Activity Relationship Models. *J. Mol. Graph. Model.* **2017**, *71*, 1-12, DOI: 10.1016/j.jmgm.2016.10.012.
- [28] Clark, M.; Cramer, R. D.; Opdenbosch, N., Van Validation of the General Purpose Tripos 5.2 Force Field. *J. Comput. Chem.* **1989**, *10*, 982-1012. DOI: <https://doi.org/10.1002/jcc.540100804>.
- [29] Burkert, U.; Allinger, N. L.; Wold, S.; Ruhe, A.; Wold, H.; Dunn, W. J.; Simon, Z.; Badileuscu, I.; Racovitan, T.; Dragomir, N., *et al.* Quantitative Approaches to Drug Design; Springer-Verlag, **1988**, Vol. 110.
- [30] Caballero, J.; Tundidor-Camba, A.; Fernández, M. Modeling of the Inhibition Constant (K_i) of Some Cruzain Ketone-Based Inhibitors Using 2D Spatial Autocorrelation Vectors and Data-Diverse Ensembles of Bayesian-Regularized Genetic Neural Networks. *QSAR Comb. Sci.* **2007**, *26*, 27-40, DOI: 10.1002/qsar.200610001.
- [31] El Aissouq, A.; Toufik, H.; Stitou, M.; Ouammou, A.; Lamchouri, F. In Silico Design of Novel Tetra-Substituted Pyridinylimidazoles Derivatives as c-Jun N-Terminal Kinase-3 Inhibitors, Using 2D/3D-QSAR Studies, Molecular Docking and ADMET Prediction.

- Int. J. Pept. Res. Ther.* **2020**, *26*, 1335-1351, DOI: 10.1007/s10989-019-09939-8.
- [32] El Aissouq, A.; Chedadi, O.; Kasmi, R.; Elmchichi, L.; En-nahli, F.; Goudzal, A.; Bouachrine, M.; Ouammou, A.; Khalil, F., Molecular Modeling Studies of C-Glycosylfavone Derivatives as GSK-3 β Inhibitors Based on QSAR and Docking Analysis. *J. Solution Chem.* **2021**, *50*, 808-822, DOI: 10.1007/s10953-021-01083-6.
- [33] Zhang, X.; Mao, J.; Li, W.; Koike, K.; Wang, J. Improved 3D-QSAR Prediction by Multiple-Conformational Alignment: A Case Study on PTP1B Inhibitors. *Comput. Biol. Chem.* **2019**, *83*, DOI: 10.1016/j.compbiolchem.2019.107134.
- [34] Ai, Y.; Wang, S. T.; Sun, P. H.; Song, F. J., Combined 3D-QSAR Modeling and Molecular Docking Studies on Pyrrole-Indolin-2-Ones as Aurora A Kinase Inhibitors. *Int. J. Mol. Sci.* **2011**, *12*, 1605-1624, DOI: 10.3390/ijms12031605.
- [35] Abraham, M. J.; Murtola, T.; Schulz, R.; Páll, S.; Smith, J. C.; Hess, B.; Lindah, E., GROMACS: High Performance Molecular Simulations through Multi-Level Parallelism from Laptops to Supercomputers. *SoftwareX* **2015**, *1-2*, 19-25, DOI: 10.1016/J.SOFTX.2015.06.001.
- [36] Best, R. B.; Zhu, X.; Shim, J.; Lopes, P. E. M.; Mittal, J.; Feig, M.; Mackerell, A. D., Optimization of the Additive CHARMM All-Atom Protein Force Field Targeting Improved Sampling of the Backbone ϕ , ψ and Side-Chain χ 1 and χ 2 Dihedral Angles. *J. Chem. Theory Comput.* **2012**, *8*, 3257-3273, DOI: <https://doi.org/10.1021/ct300400x>.
- [37] Vanommeslaeghe, K.; Hatcher, E.; Acharya, C.; Kundu, S.; Zhong, S.; Shim, J.; Darian, E.; Guvench, O.; Lopes, P.; Vorobyov, I.; Charmm, A. D. M. J., General Force Field: A Force Field for Drug-Like Molecules Compatible with the CHARMM All-Atom Additive Biological Force Fields. *J. Comput. Chem.* **2010**, *31*, 671-690, DOI: <https://doi.org/10.1002/jcc.21367>.
- [38] Jorgensen, W. L.; Chandrasekhar, J.; Madura, J. D.; Impey, R. W.; Klein, M. L.; Jorgensen, W. L.; Chandrasekhar, J.; Madura, J. D.; Impey, R. W.; Klein, M. L., Comparison of Simple Potential Functions for Simulating Liquid Water Comparison of Simple Potential Functions for Simulating Liquid Water. *J. Chem. Phys.* **1983**, *926*, DOI: 10.1063/1.445869.
- [39] Benso, B.; Bustos, D.; Zarraga, M. O.; Gonzalez, W.; Caballero, J.; Brauchi, S., Chalcone Derivatives as Non-Canonical Ligands of TRPV1. *Int. J. Biochem. Cell Biol.* **2019**, *112*, 18-23, DOI: 10.1016/J.BIOCEL.2019.04.010.
- [40] Pereira, G. J. V.; Tavares, M. T.; Azevedo, R. A.; Martins, B. B.; Cunha, M. R.; Bhardwaj, R.; Cury, Y.; Zambelli, V. O.; Barbosa, E. G.; Hediger, M. A., *et al.* Capsaicin-like Analogue Induced Selective Apoptosis in A2058 Melanoma Cells: Design, Synthesis and Molecular Modeling. *Bioorganic Med. Chem.* **2019**, *27*, 2893-2904, DOI: 10.1016/j.bmc.2019.05.020.
- [41] Aissouq, A. El; Chedadi, O.; Bouachrine, M.; Khalil, F., Development of Novel Monoamine Oxidase B (MAO-B) Inhibitors by Combined Application of Docking-Based Alignment, 3D-QSAR, ADMET Prediction, Molecular Dynamics Simulation, and MM _ GBSA Binding Free Energy. *Journal of Biomolecular Structure and Dynamics* **2022**, *0*, 1-14, DOI: 10.1080/07391102.2022.2071341.
- [42] Roth, H. S.; Botham, R. C.; Schmid, S. C.; Fan, T. M.; Dirikolu, L.; Hergenrother, P. J., Removal of Metabolic Liabilities Enables Development of Derivatives of Procaspase-Activating Compound 1 (PAC-1) with Improved Pharmacokinetics. *Journal of Medicinal Chemistry*, **2015**, *58*, 4046-4065, DOI: 10.1021/acs.jmedchem.5b00413.